Preservation of pristine Bi_2Te_3 thin film topological insulator surface after ex situ mechanical removal of Te capping layer

C. I. Fornari, P. H. O. Rappl, S. L. Morelhão, T. R. F. Peixoto, H. Bentmann, F. Reinert, and E. Abramof

Citation: APL Materials **4**, 106107 (2016); doi: 10.1063/1.4964610
View online: https://doi.org/10.1063/1.4964610
View Table of Contents: http://aip.scitation.org/toc/apm/4/10
Published by the American Institute of Physics

Articles you may be interested in

Protective capping of topological surface states of intrinsically insulating Bi_2Te_3
AIP Advances **5**, 097139 (2015); 10.1063/1.4931038

Characterizing the structure of topological insulator thin films
APL Materials **3**, 083303 (2015); 10.1063/1.4926455

Structural properties of Bi_2Te_3 topological insulator thin films grown by molecular beam epitaxy on (111) BaF_2 substrates
Journal of Applied Physics **119**, 165303 (2016); 10.1063/1.4947266

Controlled removal of amorphous Se capping layer from a topological insulator
Applied Physics Letters **105**, 241605 (2014); 10.1063/1.4904803

The quantum spin Hall effect and topological insulators
Physics Today **63**, 33 (2010); 10.1063/1.3293411

Stability of low-carrier-density topological-insulator Bi_2Se_3 thin films and effect of capping layers
APL Materials **3**, 091101 (2015); 10.1063/1.4931767

Preservation of pristine Bi_2Te_3 thin film topological insulator surface after *ex situ* mechanical removal of Te capping layer

C. I. Fornari,[1,a] P. H. O. Rappl,[1] S. L. Morelhão,[2] T. R. F. Peixoto,[3] H. Bentmann,[3] F. Reinert,[3] and E. Abramof[1]
[1]*Instituto Nacional de Pesquisas Espaciais, CP 515, 12245-970 São José dos Campos, SP, Brazil*
[2]*Instituto de Física, Universidade de São Paulo, CP 66318, 05315-970 São Paulo, SP, Brazil*
[3]*Experimentelle Physik VII, Universität Würzburg, Am Hubland, 97074 Würzburg, Germany*

(Received 19 August 2016; accepted 27 September 2016; published online 10 October 2016)

Ex situ analyses on topological insulator films require protection against surface contamination during air exposure. This work reports on a technique that combines deposition of protective capping just after epitaxial growth and its mechanical removal inside ultra-high vacuum systems. This method was applied to Bi_2Te_3 films with thickness varying from 8 to 170 nm. Contrarily to other methods, this technique does not require any sputtering or thermal annealing setups installed inside the analyzing system and preserves both film thickness and surface characteristics. These results suggest that the technique presented here can be expanded to other topological insulator materials. © *2016 Author(s). All article content, except where otherwise noted, is licensed under a Creative Commons Attribution (CC BY) license (http://creativecommons.org/licenses/by/4.0/).* [http://dx.doi.org/10.1063/1.4964610]

V-VI compounds, like Bi_2Te_3, Bi_2Se_3, and Sb_2Te_3, belong to a new class of materials called three-dimensional topological insulators (TIs), which exhibit insulating characteristics inside the bulk and gapless metallic states on the surface.[1–4] The topological properties of bismuth chalcogenides have been theoretically predicted[3,5] and the conducting surface states, consisting of a single Dirac cone at the Γ point, have been experimentally confirmed by angle resolved photoelectron spectroscopy (ARPES) measurements in bulk crystals.[6–9] In these experiments fresh surfaces are obtained by cleaving the bulk crystals inside the ARPES ultra-high vacuum (UHV) chamber. To inhibit bulk conduction, extrinsic counter doping (Ca for Bi_2Se_3[7] and Sn for Bi_2Te_3[9]) has been used to tune the Fermi level inside the band gap in a position where it crosses only the surface states, obtaining an insulating bulk behavior. However, even in UHV conditions the properties of the surface states degrade on a time scale of hours.[9]

Molecular beam epitaxy (MBE) has been applied to grow thin films of bismuth chalcogenides presenting high crystalline quality and well controlled properties on different substrates.[10] Intrinsic conduction only through the topological surface states has been achieved on these films by carefully controlling the MBE growth kinetics.[11–13] All these experiments have been performed on thin films directly transferred after growth from the MBE system into the ARPES measurement chamber through UHV lines. Air exposure of the topological insulator crystals leads to the formation of oxide layers.[14] This oxidation process degrades the TI surface, making *ex situ* surface analysis unfeasible, which hinders the characterization of TI materials using other techniques at different facilities, including synchrotron based end-stations. Therefore, different methods have been proposed to protect the surface of TI films for *ex situ* surface measurements.

One method consists of removing the oxidized layer through Ar^+ ion sputtering followed by thermal annealing to reconstruct the sample surface.[15,16] Although this method enables ARPES measurements, the sputtering process usually leads to rough or damaged surfaces and stoichiometry

[a]Author to whom correspondence should be addressed. Electronic mail: celso.fornari@inpe.br. Tel.: +55 12 3208-6681.

 ©Author(s) 2016.

can be modified during annealing due to Te or Se re-evaporation. In addition, this method is not appropriate to clean heavily oxidized film surfaces.[17]

A second technique employs the deposition of a protective Te or Se capping on the bismuth chalcogenide films just after the MBE growth. After transferring the capped sample to the *ex situ* UHV measuring system, passing through unavoidable air exposure, these protective cappings have to be removed to restore the film surface. Thermal desorption inside the UHV chamber is the most used procedure and consists of elevating the sample temperature until the film surface is completely exposed. Se capping is preferably used due to its low desorption temperature, but it normally changes the surface stoichiometry of Te-based TI compounds during thermal decapping.[18,19] Refinements of this technique have shown that it is possible to restore pristine surfaces after thermal removal of sputtered Se capping on Bi_2Se_3, which was exposed to air for a few hours[20] or thermal desorption of ultra-thin Te capping on Bi_2Te_3 films after exposition to air for 5 min.[21]

A third technique applied to layered van der Waals materials consists of cleaving thin films (thicker than 50 nm) inside the UHV chamber to remove the oxidized surface, exposing a new fresh surface to perform the aimed analysis.[17] However, this procedure changes both film thickness and surface morphology, leading to uncontrollable parameters for surface characterization.

This work presents a technique that combines the deposition of a protective capping layer after the epitaxial growth with its mechanical removal inside the UHV chamber for *ex situ* surface investigation. The idea is to apply the adhesive tape technique, commonly used to cleave bulk crystals, for removing the cap layers to expose fresh surfaces. This method is applied here to Te capped bismuth telluride films with varied film and cap thicknesses. The Te cap is completely removed by the adhesive tape, exposing an unaltered surface without changing the Bi_2Te_3 film thickness. Analyses performed on the exposed films prepared by the method described here demonstrate that a pristine Bi_2Te_3 surface is totally preserved, exhibiting protected topological surface states of intrinsically insulating Bi_2Te_3, as reported for as-grown films measured *in situ* without breaking vacuum.[11–13] It is important to emphasize that the *ex situ* UHV surface analyses were performed after keeping the samples at room conditions during 3 months.

Bismuth telluride epitaxial films were grown in a Riber 32P MBE system on freshly cleaved (111) BaF_2 substrates, which have a lattice mismatch of only 0.04% to Bi_2Te_3, see Figs. 1(a) and 1(b). A nominal Bi_2Te_3 solid source, which determines the growth rate, and two extra Te cells, to compensate the loss of tellurium during growth, were used. The beam equivalent pressure (BEP) of Bi_2Te_3 and Te fluxes were measured by a Bayer-Alpert ion gauge and the Te to Bi_2Te_3 BEP ratio was adjusted according to the substrate temperature to obtain single phase Bi_2Te_3 films. For the samples investigated here, the substrate temperature ranged from 240 °C to 270 °C and the BEP ratio

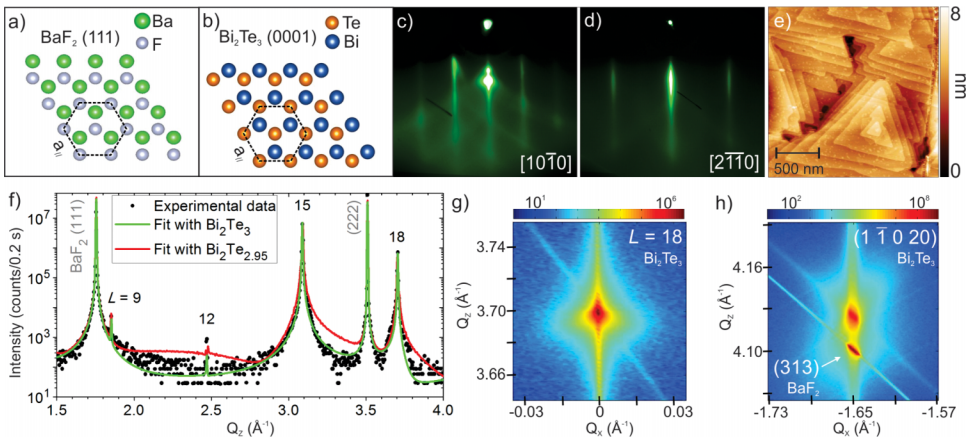

FIG. 1. Surface lattices of (a) cubic BaF_2 (111) plane and (b) hexagonal Bi_2Te_3 (0001) plane. Structural characterization of a 150 nm Bi_2Te_3/BaF_2 film: ((c) and (d)) RHEED patterns along two symmetry azimuths acquired just after growth; (e) *Ex situ* AFM surface image; (f) Q_Z-scan measured along the growth direction together with two calculated x-ray diffraction curves for pure Bi_2Te_3 (blue line) and Bi-richer $Bi_2Te_{2.95}$ (red line) phases. Reciprocal space maps of (g) symmetric $L = 18$ Bi_2Te_3 and (h) asymmetric $(1\bar{1}020)$ Bi_2Te_3 and (313) BaF_2 Bragg peaks.

from 1 to 3. A growth rate of approximately 1 nm/min was used and the deposition time was set to obtain Bi_2Te_3 films with thickness from 8 to 170 nm. Details about MBE growth of these films can be found elsewhere.[22] To protect the films for the *ex situ* UHV surface analyses, Te capping layers were deposited just after growth at a substrate temperature around 30 °C with a deposition rate of 6 nm/min. The thickness of the protective cap ranged from 100 to 200 nm.

To monitor *in situ* the film surface during growth, reflection high-energy electron diffraction (RHEED) patterns were acquired using a 35 keV RHEED system. The RHEED analysis indicated a layer-by-layer growth mode since the early stages of bismuth telluride epitaxy on (111) BaF_2 substrates.[22] Figs. 1(c) and 1(d) show streaky RHEED patterns along two symmetry azimuths in a 150 nm Bi_2Te_3 film surface just after growth, evidencing a highly ordered film. *Ex situ* atomic force microscopy (AFM) images were taken to evaluate surface morphology using a Veeco SPM Multimode in tapping mode. AFM image of this film, displayed in Fig. 1(e), exhibits the spiral-like triangular domains, which reflects the threefold symmetry of Fig. 1(b), with terraces steps of 1 nm in height corresponding to one quintuple layer (QL) of Bi_2Te_3.

X-ray diffraction was measured at the XRD2 beamline of the Brazilian Synchrotron Light Laboratory (LNLS) with a photon energy of 8004 eV (λ = 1.54904 Å). The Q_z-scan measured along [0001] film direction is plotted in the graph of Fig. 1(f). Besides the (111) and (222) BaF_2 substrate peaks, only the (000L) Bi_2Te_3 Bragg peaks with $L = 3n$ (n = integer) are observed, as expected for epitaxy with the Bi_2Te_3 (0001) hexagonal plane parallel to the BaF_2 (111) surface. Fig. 1(f) also plots two diffraction curves calculated using a set of recursive equations[23] and fitted to the experimental data considering a pure Bi_2Te_3 and a Bi-richer $Bi_2Te_{2.95}$ phase. It evidences that a pure phase Bi_2Te_3 film is obtained. Reciprocal space maps (RSMs) measured in the vicinity of the symmetric (00018) and the asymmetric $(1\bar{1}020)$ Bi_2Te_3 reciprocal lattice points are shown in Figs. 1(g) and 1(h), respectively. In both RSMs, scattering along the crystal truncation rod, parallel to Q_z, and along the Ewald sphere surface (oblique streaks perpendicular to the diffracted wavevectors) are visible. The low scattering in the in-plane direction Q_x on the RSM around $L = 18$ peak indicates a film with low mosaicity and a small density of structural defects, demonstrating that the Bi_2Te_3 thin films grown here are of very high structural quality. In Fig. 1(h), the asymmetrical $(1\bar{1}020)$ Bi_2Te_3 epilayer and (313) BaF_2 substrate reciprocal lattice points are well aligned along the crystal truncation rods, i.e., their maxima are in the same Q_x position, indicating that the epilayer hexagonal lattice is perfectly matched to the substrate cubic lattice.

The Te capped samples and the decapping procedure are investigated *ex situ* at room conditions by cross section images acquired using a TESCAN MIRA3 field-emission gun (FEG) microscope, AFM surface images, and x-ray reflectivity curves measured in a PANalytical X'Pert MRD high-resolution x-ray diffractometer. Fig. 2(a) shows a FEG microscopy cross section image of a 25 nm thick Bi_2Te_3 film capped with a 100 nm Te layer. To illustrate the method proposed here, a schematic diagram of the mechanical removal technique using adhesive tape is depicted in Fig. 2(b). The sample is glued to a holder and an adhesive tape is attached to the cap surface. The capping layer can be removed either by pulling the tape or by fixing the adhesive tape and moving the holder. Fig. 2(c) exhibits the AFM surface image of the 25 nm Bi_2Te_3 film just after removing the Te cap layer. For comparison, the surface of a non-capped Bi_2Te_3 film grown at the same conditions and with the same thickness is shown in the AFM image of Fig. 2(d). These images demonstrate that the film surface is completely preserved after the cap removal, exhibiting the same terraced triangular domains.

Fig. 2(e) shows the x-ray reflectivity curves of a 50 nm Bi_2Te_3 film covered with 100 nm of Te protective cap before (bottom curve) and after (top curve) decapping procedure. The reflectivity curve before decapping exhibits interference fringes from the cap layer at lower angles followed by fringes due to the Bi_2Te_3 film at higher angles. After cap removal, only the interference fringes from the Bi_2Te_3 film are visible. The red solid lines correspond to the calculated curves that best fitted to the experimental data. The thickness (t) and roughness (σ) values obtained by fitting indicate that the film thickness and flatness are totally preserved by the cap layer removing method described here. Since the films surface are terminated in complete QLs and the protective cap is grown at room temperature with high deposition rates, no ionic bonds between the Te cap and the film surface are expected. The weak coupling between the uppermost Te^1 monolayer of the QL and the Te atoms from the capping facilitates the removal of the protective cap exactly at the film/cap interface.

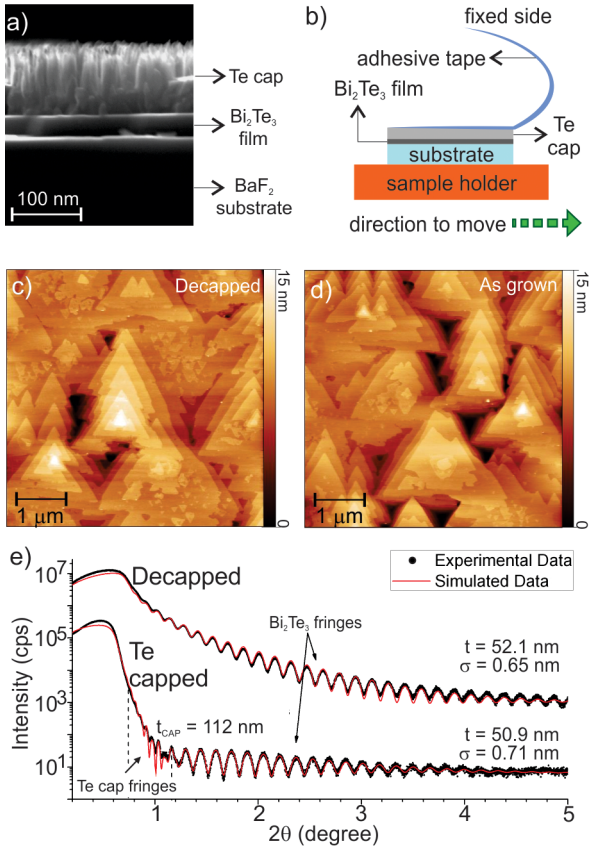

FIG. 2. (a) Cross section FEG microscopy image of a capped Bi_2Te_3 film. (b) Schematic diagram of the cap layer removal technique. AFM surface images of (c) decapped and (d) as-grown 25 nm thick Bi_2Te_3 films. (e) X-ray reflectivity of a 50 nm Bi_2Te_3 film covered with 100 nm Te protective capping before (lower curve) and after (upper curve) decapping procedure. Red solid lines are calculated curves that best fitted to the data, giving accurate layer thickness (t) and surface roughness (σ).

To characterize the exposed film surface after removing the Te cap layer in UHV conditions, an integrated UHV surface analysis system composed of low-energy electron diffraction (LEED) from Omicron, x-ray photoelectron spectroscopy (XPS), and ARPES facilities was used. The photoelectron experiments were performed at room temperature with a Scienta R4000 hemispherical analyzer using He I_α radiation (21.2 eV) with a resolution of 15 meV for ARPES and the Al K_α emission line (1486.7 eV) for XPS measurements.

The protective cappings were removed by fixing the adhesive tape to the wall of the load-lock chamber (pressure $\sim 5 \times 10^{-8}$ Torr) and transferring the sample holder to the measurement chamber (pressure $\sim 5 \times 10^{-11}$ Torr). Figs. 3(a) and 3(b) show the LEED images of a 150 nm Bi_2Te_3 film acquired at 50 and 67 eV, respectively. Bright spots forming the hexagonal pattern characteristic of the crystal surface threefold symmetry are clearly visible in both images, demonstrating that an intact Bi_2Te_3 surface is completely exposed. The XPS spectrum of the freshly exposed Bi_2Te_3 film surface presents only the peaks corresponding to Te and Bi core levels and their plasmon satellites, indicating the absence of contaminants on the surface after Te capping removal. In particular, even at higher emission angles there is no signal from the Te capping which appears at characteristic binding energies of 585 and 575 eV for Te $3d_{3/2}$ and $3d_{5/2}$, respectively. The Te 3d and Bi 4f core levels XPS peaks, shown in Fig. 3(c), are very narrow and symmetric, evidencing no excess of Te or Bi.

ARPES spectrum in the vicinity of $\bar{\Gamma}$ point of a Bi_2Te_3 fresh surface recorded just after the Te cap removal is shown in Fig. 4(a). In addition to the M-shaped bulk valence band (BVB), the linear dispersion of the topological surface states (TSS) is clearly visible, evidencing the massless Dirac fermions.[9] In this ARPES spectrum, the Fermi level lies inside the band gap intersecting only the TSS, which is an indication of a bulk insulating film. The Dirac point is located 205 meV

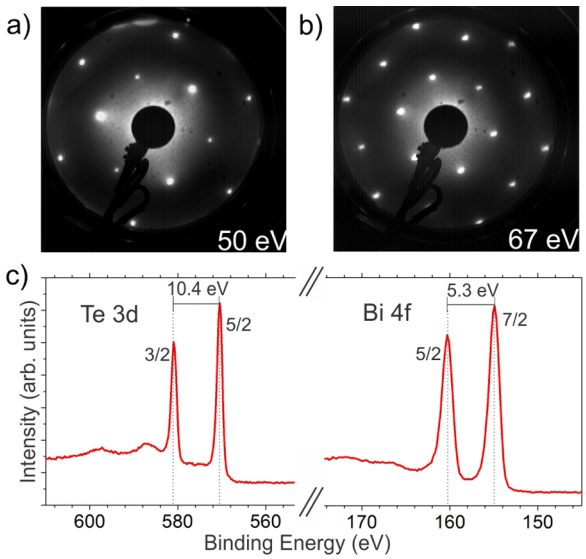

FIG. 3. Surface analysis of a 150 nm Bi_2Te_3 epilayer after Te cap removal inside UHV chamber: ((a) and (b)) LEED images measured at different photon energies showing clearly the Bi_2Te_3 hexagonal surface pattern. (c) XPS spectrum exhibiting the Te 3d and Bi 4f core levels and their plasmon satellites, indicating a completely preserved film surface.

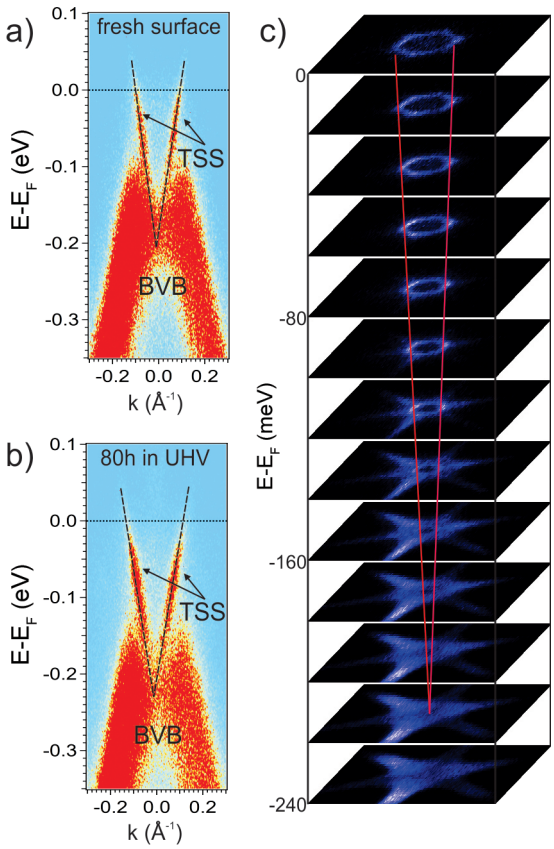

FIG. 4. ARPES spectrum near the $\bar{\Gamma}$ point of a 150 nm Bi_2Te_3 film surface acquired (a) just after removal of Te protective layer and (b) after 80 h in UHV conditions. (c) Constant energy maps obtained at different binding energies for this sample after 24 h inside the UHV chamber.

below the Fermi level and the obtained Fermi velocity is 2.2 eV·Å (3.3×10^5 m/s), which is very close to the values obtained for an intrinsic Bi_2Te_3 topological insulating thin film.[13] These results demonstrate that the technique presented here is very effective to protect the surface of topological insulators from contamination during air exposure, preserving the TSS. Fig. 4(b) shows the ARPES spectrum measured after keeping this sample at UHV environment during 80 h. After this period, the Dirac point shifted downwards to 230 meV below the Fermi level, indicating that the bulk conduction band starts to be populated due to the residual gas atoms adsorbed on the surface. Fig. 4(c) displays the constant energy contour maps at different binding energies from the Fermi level to the BVB for this Bi_2Te_3 epitaxial film measured 24 h after decapping. The Fermi surface, visible in the uppermost layer of the map, exhibits the TSS hexagonal warping characteristic of the Bi_2Te_3 material. This warping becomes less pronounced as the binding energy increases passing along the Dirac cone (represented by red lines) in the direction of the BVB, and for binding energies higher than 100 meV, the BVB contribution starts to be visible.

In summary, the mechanical removal of Te capping layers on Bi_2Te_3 films by using adhesive tape proved to be a simple and robust technique to expose pristine surfaces for *ex situ* analyses. In contrast to other methods, this technique preserves film thickness, surface morphology, and stoichiometry, and does not require sputtering and/or thermal annealing facilities inside *ex situ* UHV analysis systems. It was possible to observe topological surface states of intrinsically bulk insulating films when applying this capping removal method to Bi_2Te_3 films grown at optimized conditions. These results suggest that the technique proposed here can be applied to other topological insulator materials with different protective layers.

The authors wish to thank Sebastian Fiedler for valuable discussions. The authors acknowledge CNPq (Grant Nos. 142191/2014-0, 302134/2014-0, 307933/2013-0, and 306982/2012-9), FAPESP (Grant No. 2014/04150-0), DFG via SFB1170 (Project No. A01) for financial support, and LNLS (Proposal No. XRD2-20150037) for measurement assistance.

[1] M. Z. Hasan and C. L. Kane, Rev. Mod. Phys. **82**, 3045 (2010).
[2] Y. Ando, J. Phys. Soc. Jpn. **82**, 102001 (2013).
[3] L. Fu and C. L. Kane, Phys. Rev. B **76**, 045302 (2007).
[4] J. E. Moore, Nature **464**, 194 (2010).
[5] H. Zhang, C.-X. Liu, X.-L. Qi, X. Dai, Z. Fang, and S.-C. Zhang, Nat. Phys. **5**, 438 (2009).
[6] Y. Xia, D. Qian, D. Hsieh, L. Wray, A. Pal, H. Lin, A. Bansil, D. Grauer, Y. S. Hor, R. J. Cava, and M. Z. Hasan, Nat. Phys. **5**, 398 (2009).
[7] D. Hsieh, Y. Xia, D. Qian, L. Wray, J. H. Dil, F. Meier, J. Osterwalder, L. Patthey, J. G. Checkelsky, N. P. Ong, A. V. Fedorov, H. Lin, A. Bansil, D. Grauer, Y. S. Hor, R. J. Cava, and M. Z. Hasan, Nature **460**, 1101 (2009).
[8] D. Hsieh, Y. Xia, D. Qian, L. Wray, F. Meier, J. Dil, J. Osterwalder, L. Patthey, A. Fedorov, H. Lin, A. Bansil, D. Grauer, Y. S. Hor, R. Cava, and M. Z. Hasan, Phys. Rev. Lett. **103**, 146401 (2009).
[9] Y. L. Chen, J. G. Analytis, J.-H. Chu, Z. K. Liu, S.-K. Mo, X. L. Qi, H. J. Zhang, D. H. Lu, X. Dai, Z. Fang, S. C. Zhang, I. R. Fisher, Z. Hussain, and Z.-X. Shen, Science **325**, 178 (2009).
[10] L. He, X. Kou, and K. L. Wang, Phys. Status Solidi RRL **7**, 50 (2013).
[11] G. Wang, X.-G. Zhu, Y.-Y. Sun, Y.-Y. Li, T. Zhang, J. Wen, X. Chen, K. He, L.-L. Wang, X.-C. Ma, J.-F. Jia, S. B. Zhang, and Q.-K. Xue, Adv. Mater. **23**, 2929 (2011).
[12] J. J. Lee, F. T. Schmitt, R. G. Moore, I. M. Vishik, Y. Ma, and Z. X. Shen, Appl. Phys. Lett. **101**, 013118 (2012).
[13] K. Hoefer, C. Becker, D. Rata, J. Swanson, P. Thalmeier, and L. H. Tjeng, Proc. Natl. Acad. Sci. U. S. A. **111**, 14979 (2014).
[14] H. Bando, K. Koizumi, Y. Oikawa, K. Daikohara, V. A. Kulbachinskii, and H. Ozaki, J. Phys.: Condens. Matter **12**, 5607 (2000).
[15] J. Krumrain, G. Mussler, S. Borisova, T. Stoica, L. Plucinski, C. M. Schneider, and D. Grützmacher, J. Cryst. Growth **324**, 115 (2011).
[16] L. Plucinski, G. Mussler, J. Krumrain, A. Herdt, S. Suga, D. Grützmacher, and C. M. Schneider, Appl. Phys. Lett. **98**, 222503 (2011).
[17] S. E. Harrison, B. Zhou, Y. Huo, A. Pushp, A. J. Kellock, S. S. P. Parkin, J. S. Harris, Y. Chen, and T. Hesjedal, Appl. Phys. Lett. **105**, 121608 (2014).
[18] H. Maaß, S. Schreyeck, S. Schatz, S. Fiedler, C. Seibel, P. Lutz, G. Karczewski, H. Bentmann, C. Gould, K. Brunner, L. W. Molenkamp, and F. Reinert, J. Appl. Phys. **116**, 193708 (2014).
[19] K. Virwani, S. E. Harrison, A. Pushp, T. Topuria, E. Delenia, P. Rice, A. Kellock, L. Collins-McIntyre, J. Harris, T. Hesjedal, and S. Parkin, Appl. Phys. Lett. **105**, 241605 (2014).
[20] J. Dai, W. Wang, M. Brahlek, N. Koirala, M. Salehi, S. Oh, and W. Wu, Nano Res. **8**, 1222 (2015).
[21] K. Hoefer, C. Becker, S. Wirth, and L. Hao Tjeng, AIP Adv. **5**, 097139 (2015).
[22] C. I. Fornari, P. H. O. Rappl, S. L. Morelhão, and E. Abramof, J. Appl. Phys. **119**, 165303 (2016).
[23] S. L. Morelhão, *Computer Simulation Tools for X-ray Analysis* (Springer International Publishing, Cham, 2016).